

Article

# Photogrammetric Investigation of Storm-Induced Erosion Process on Sandy Beach Profile in Medium-Scale Flume

Jun Wang<sup>1,2</sup>, Bo Yang<sup>2,\*</sup> , Bingchen Liang<sup>2</sup>, Zai-Jin You<sup>1,3</sup> , Zhenlu Wang<sup>2</sup>  and Zhaowei Wang<sup>1</sup> 

<sup>1</sup> Centre for Ports and Marine Safety, Dalian Maritime University, Dalian 116024, China; wangjun2021@dlnu.edu.cn (J.W.); b.you@dlnu.edu.cn (Z.-J.Y.); wzw1128@dlnu.edu.cn (Z.W.)

<sup>2</sup> College of Engineering, Ocean University of China, Qingdao 266100, China; bingchen@ouc.edu.cn (B.L.); wangzhenlu@ouc.edu.cn (Z.W.)

<sup>3</sup> School of Civil Engineering, University of Queensland, Brisbane, QLD 4072, Australia

\* Correspondence: yangbo1011@ouc.edu.cn; Tel.: +86-15610053125

**Abstract:** In this study, laboratory experiments were conducted to investigate the influence of changes in storm wave height and water level on beach response in a medium-scale wave flume. A schematic storm was simulated (rising, apex, and waning phases). A non-intrusive photogrammetric method was used to collect high-resolution and synchronous data regarding the free surface water elevation and bed level, from which shoreline location, sandbar position, cross-shore sediment transport rates, and nonlinear wave parameters were derived. The cross-shore sediment transport was in agreement with previous laboratory measurements, including the monotonous exchange from foreshore erosion to shoaling zone accretion in most stages of the storm simulation. The surf zone was the main region supplying sediment for beach morphology modification and sandbar generation. The degree of storm erosion was not completely determined by the largest wave height and water level or the cumulative wave power of the apex phase. The largest gradients of the wave parameter sequence change occurred in the rising phase, and this was the main factor generating efficient beachface erosion. It induced an increase in sandbar size, accompanied by the cross-shore motion of maximum velocity amplitude, more violent disturbances of wave nonlinearity, and increased surf zone erosion, with these factors increasing beach instability and leading to more severe storm erosion. The large wave height and water level resulted in shoreline retreat, with a more significant swash zone erosion under a higher runup. The offshore sediment transport turned toward the onshore direction as the original large sandbar deteriorated under the decreasing wave parameter sequence in the waning phase.

**Keywords:** laboratory experiment; wave breaking; wave parameter sequence; storm erosion; sandbar; cross-shore sediment transport



**Citation:** Wang, J.; Yang, B.; Liang, B.; You, Z.-J.; Wang, Z.; Wang, Z.

Photogrammetric Investigation of Storm-Induced Erosion Process on Sandy Beach Profile in Medium-Scale Flume. *J. Mar. Sci. Eng.* **2024**, *12*, 518. <https://doi.org/10.3390/jmse12030518>

Academic Editor: Enzo Pranzini

Received: 27 February 2024

Revised: 18 March 2024

Accepted: 19 March 2024

Published: 21 March 2024



**Copyright:** © 2024 by the authors. Licensee MDPI, Basel, Switzerland. This article is an open access article distributed under the terms and conditions of the Creative Commons Attribution (CC BY) license (<https://creativecommons.org/licenses/by/4.0/>).

## 1. Introduction

Storm events can significantly impact the morphology of sandy beaches, leading to beach erosion and inundation as the sequences of increasing wave heights and sea levels elevate the mean water surface and wave runup. The accompanying extremely energetic coastal wave conditions significantly impede coastal economic development. The impact of storm events on coastal morphodynamics is attracting increasing interest from the scientific community. However, there has been no systematic overview of cross-shore sediment transport during a sequence of changes in storm wave parameters, and there are still some challenges in how a beach responds to different storm phase sequences and the main disaster-causing factors in a storm.

Storm surges and large wave heights are considered to be the watermain characteristics of extreme climate events. Surface-induced turbulence, especially wave-velocity nonlinearities [1–4], such as wave shoaling, wave breaking, and bore collapse, play an important role in stirring up bottom sediment and aggravating imbalances in cross-shore sediment transport, which trigger potentially rapid beach erosion. The rise in sea level during storm

surges results in the break point of high waves moving further onshore. The subsequent strong wave nonlinear induced turbulence and wave runups promote beachface erosion and result in significant and substantial modifications to beach morphology [5–7]. The ongoing morphodynamic evolution of beaches under wave forcing is influenced by various factors, including large coastal waves, high levels of turbulence in nonlinear hydrodynamic processes, and the combined effects of storm surges and real-time changes in wave forcing. These influences result in the migration of breaking points, with variations in sediment transport both toward and away from the breaking point, consequently contributing to beach instability and changes in cross-shore sediment transport.

Over the last decades, laboratory and field studies have been carried out to advance the investigation of sediment transport processes during coastal storm events. Based on observations from along the New South Wales coast, the problems of coastal hazard tend to be exacerbated due to the potential changes in storm, extreme wave events and rising sea levels [8]. A large amount of coastal sediment could be eroded in a short time; most of the erosion sediment becomes irreversible after a storm [9,10]. Field observations prove that the shoreline of a beach could retreat up to 50 m by removing foreshore sediment and depositing it offshore after an extreme storm [11,12]. Typically, most relevant studies are mainly about field observations before and after a storm; studies measuring the influence of changing storm wave parameters on beach response are rare because harsh conditions often preclude observations [13,14]. Aagaard et al. [15] innovatively studied cross-shore sediment transport processes on the shoreface of a reflective beach including pre-, during-, and post-storm conditions via new field measurements observed at Pearl Beach. Nevertheless, consistent with earlier field surveys, the detailed process of beach morphodynamic evolution as wave parameters change during a storm could not be illustrated because of the long time span and coarse spatial resolution of the field data. Additionally, Larsen et al. [16] mentioned that the limited availability of data always makes it difficult to distinguish the contributions of longshore and cross-shore sediment transport due to the inherent complexity of natural beaches. Because laboratory investigations provide a controlled environment to study the complex interactions between waves, sediment transport, and beach morphology, they allow for a better understanding of the fundamental physical mechanisms driving sandy beach evolution. Using camera image systems together with wave flumes is now considered to be a feasible method to enable real-time data collection during a storm [13,17,18]. A stereo video was successfully used in a 2D wave flume for studying the process of dune erosion and developing parameterized models [14]. By comparing the influence of three storm sequences (storm events that arrive in close temporal succession) on beach profile evolution, Eichertopf et al. [19] concluded that final morphology was mainly dependent on the end wave condition of the sequence without significant cumulative effects, and storm sequencing is preferred for determining the morphology change rate. However, studies that investigate the effects of short-term wave hydrodynamics during a storm event are scarce. Currently, the method of staged experimental simulation is an available way to explore the process of beach storm erosion due to changes in wave height and sea level during a storm event. In a staged experiment based on a schematic storm, the attack of the different storm phases was illustrated, and offshore sediment transport occurred in the apex storm phase, while the waning storm phase played a role in beach recovery by onshore sediment transport [13]. Baldock et al. [20] reported that sandbar development and relic sandbar stranding in offshore sediment transport increase the complexity of beach response to sequences of wave climates, such as the rising and waning change in wave energy that occurs during storm events, resulting in morphological hysteresis. Additionally, Polidoro et al. [21] took advantage of simulating double-peaked wave spectra to stand for the observation of extreme events from 2006 to 2014. The influence of sea level rise on nourished and non-nourished beaches was investigated in a wave flume, and the performance of the Bruun Rule or its modification by Rosati et al. [22] and the PTM model profile translation model in the prediction of shoreline recession was checked [23,24]. Beuzen et al. [25] also investigated the response of a beach profile with seawalls to rising sea levels. However,

the processes of cross-shore sediment transport under changes in the combination of wave height and sea levels during a storm have rarely been investigated.

In this study, a schematic storm with three different phases (rising, apex, and waning) was simulated step by step, considering the change in wave height and water level in a 2D wave flume. The synchronous real-time free surface water elevation and beach profiles were collected using our non-intrusive photogrammetric method, from which beach behavior (shoreline, sandbar, etc.), sediment transport rates, and wave nonlinearity transformations across the beach profile were estimated at timescales faster than surveys typically conducted in wave flumes without any interruption of wave forcing. The process of beach response to the sequence of wave height and water level change during a storm was quantitatively investigated by analyzing the beach behavior and wave hydrodynamics associated with sediment transport on a mildly sloped ( $S = 1:10$ ) sandy beach. Unlike surveys that start with piecewise planar initial beach profiles, the equilibrium beach profile after constant wave forcing was used as the initial condition.

## 2. Experimental Setup and Method

### 2.1. Wave Flume and Instrumentation

The experiments were produced in the medium-scale wave flume (30 m long, 0.6 m wide, and 1 m high) at the Ocean University of China, Qingdao, China. For a detailed arrangement of the present experiments, refer to Wang et al. [26]. In this section, only the most relevant descriptions for this thesis are shown. The changes in the waves of a schematic storm were simulated in stages from 0.1 m (calm) to 0.2 m (apex) in 0.02 m steps with a constant wave period  $T = 1.5$  s, and the corresponding water level was from 0.46 m (calm) to 0.56 m (apex) in similar steps of 0.02 m. The calm wave condition ( $H = 0.1$  m,  $T = 1.5$  s,  $d = 0.46$  m) was simulated on a planar starting slope beach profile  $S = 1:10$  for achieving the equilibrium profile, which was used as the initial beach profile for storm simulation. The shoreline and sandbar were used as indicators for determining profile stabilization and equilibrium attainment, respectively. It was observed that the rate of beach evolution under a calm wave slowed down after 4 h, arriving at a stable state. Thus, storm simulation was started on the beach profile after 4 h of calm wave action, and excluding the calm wave condition, the sequence of wave parameters during storm simulations was 0.12 to 0.2 to 0.12 m in wave height and 0.48 to 0.56 to 0.48 m in water level (detailed in Section 2.2). Well-sorted natural beach sand of  $d_{50} = 0.21$  mm was used to make the sandy beach, which was composed of a planar slope ( $S = 1:10$ ) that followed a wide berm at the back.

In addition to three side-looking industrial cameras (GS3-U3-41C6M-C, Point Gray (Canada)) for using the non-intrusive photogrammetric system (for details, see Section 2.2), five capacitor wave gauges ( $\eta_1 - \eta_5$ ) were thoroughly placed along the flume to collect the free water surface elevation from the beach toe to the seaward side of the sandbar, including the shoaling zone and outer surf zone. Data describing the further shallow region—inner surf zone and swash zone were dependent on the non-intrusive photogrammetric system. The reliability of data in the shoaling zone and outer surf zone measured using an imaging system has been proven by Wang et al. [26]. In consideration of the good performance in the shoaling zone and outer surf zone, we believe that the data from the inner surf zone and swash zone were still credible. Two acoustic Doppler velocimeters (ADV; U1-U2) were arranged at both sides of the sandbar, including the outer surf zone and inner surf zone or swash zone; these data had been described in detail by Wang et al. [27]. The sampling rates of the wave gauges and ADVs were set to 20 Hz and 50 Hz, respectively. The detailed experimental setup is shown in Figure 1.

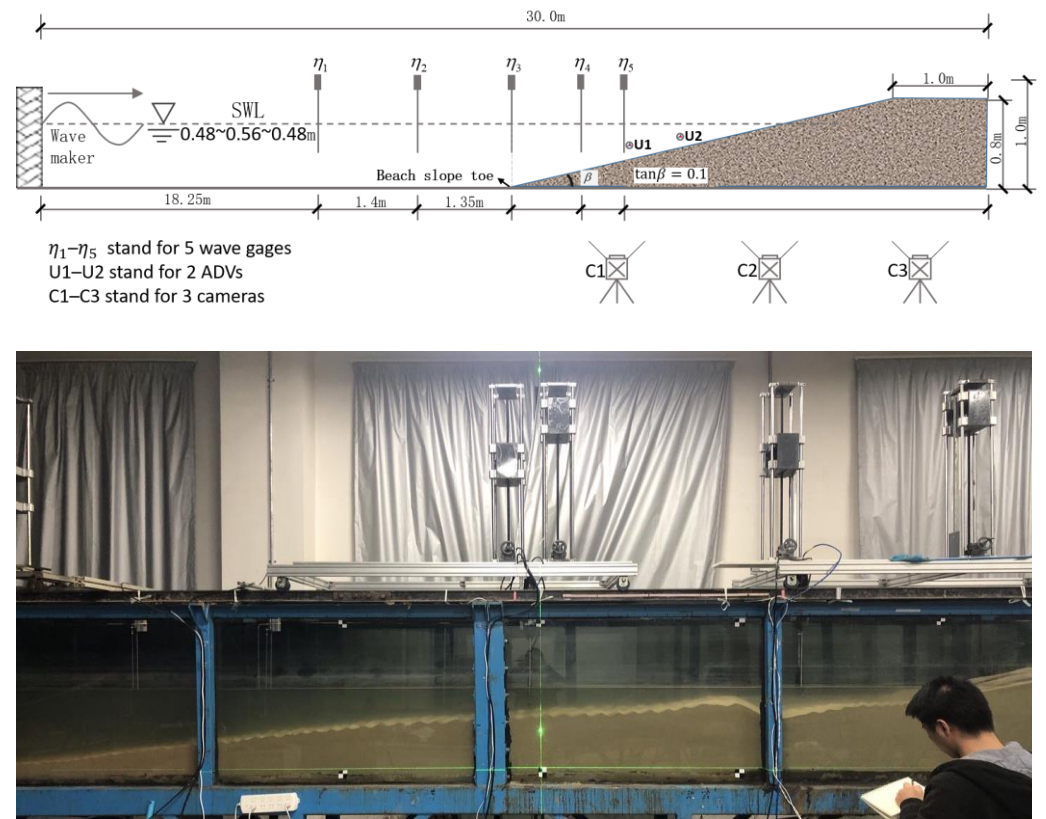


**Figure 1.** The experimental setup and instrumentation.

### 2.2. Simulation of Storm Waves

Changes in wave height and water level are considered to be the main features in a storm simulation. The duration and sequence of changes in wave parameters of the present schematic storm were designed with reference to coastal measurements made in Qingdao and the record of a storm event at Pearl Beach [28]. The extreme tidal range of a storm event could be up to 2.5 m, and the duration of a storm event is always approximately 12 h with a stage of increasing intensity as the storm arrives, then reaching the peak, and keeping stable for a period of time, before returning to calm conditions as the storm dissipates. The durations of the three storm phases were assumed to be the same length. Therefore, according to our model scale of 1:25 (time scale 1:5), the simulation range of water level change was 0.1 m, and the run time of the storm simulation was approximately 3 h. The sequence of wave height and water level change during a storm simulation followed the three-phase sequence (Figure 2). The storm rising phase was gradually increased from  $d = 0.48$  m and  $H = 0.12$  m to  $d = 0.54$  m and  $H = 0.18$  m in +0.02 m steps during a staged experiment for 60 min. In the second apex phase, the peak value condition ( $d = 0.56$  m and  $H = 0.2$  m) was kept for approximately 60 min. The final waning phase was symmetrical to the initial rising phase with the same length of 60 min, and it was gradually decreased to  $d = 0.48$  m and  $H = 0.12$  m in  $-0.02$  m steps.

The details of the storm wave simulation sequence are shown in Table 1. Because wave breaking affected the sediment mobilization rate, which is directly related to the sediment transport intensity, it has been reported that plunging breakers are more effective in entraining and mixing sediment than spilling breakers due to the different behavior of turbulence release. Higher production rates and a more rapid downward spread are found under plunging compared to spilling waves [29–32]. Anfuso [33] also concluded that the morphodynamic beach state is mainly determined by beach characteristics and breaking wave height and type. The types of wave breaking are also shown in Table 1.

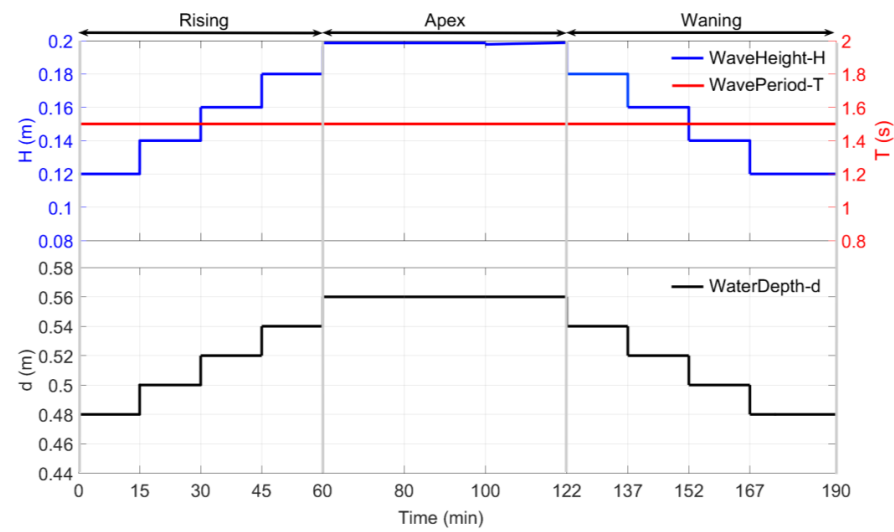


Figure 2. The sequence of changes in wave height and water level during the storm experiment.

Table 1. Wave parameter sequence during three phases of storm simulation.

Storm	$d_{50}$ (mm)	S	H (m)	T (s)	d (m)	$\zeta$	D (hr)
Rising	0.21	1:10	0.12~0.18	1.5	0.48~0.54	Spilling	1
Apex	0.21	1:10	0.2	1.5	0.56	Spilling	1
Waning	0.21	1:10	0.18~0.12	1.5	0.56~0.48	Spilling–plunging	1

### 2.3. Non-Intrusive Imaging Data Collection System

A collection system was used to continuously obtain real-time photographic images of the free water surface profile and beach profile at a fast 10 Hz sampling rate. The system consisted of three GS3-U3-41C6M-C Point Grey high-definition industrial cameras, each with a high resolution of  $2048 \times 2048$  and equipped with an HC1205A 12 mm industrial lens; light-shielding cloth covering the opposite flume glass wall; and several sunlight lamps to illuminate the water–bed interface in the wave flume to ensure that clear photographic images were obtained (for an on-site photograph, see Figure 3). Each camera was connected to a PC, and the three PCs were controlled by an intelligent synchronous controller (ISC) via USB to obtain synchronous images from each of the different cameras. The use of the Point Gray camera had the advantage of avoiding camera focusing problems in capturing images as waves run. The down-facing lamps were set up to illuminate the flume water to overcome the influence of a high sediment concentration on accessing the beach profile, especially under high suspended sediment concentrations, especially under wave breaking. In this way, images with a clearer water–bed interface were captured. The purpose of the light-shielding cloth was to diffuse light and reduce reflected light. On the basis of the camera’s observational range and frame rate, the corresponding spatial and temporal resolution was about 1.4 mm and 0.1 s, respectively.

A postprocessing analysis program was developed to improve the original lab image and recognize the interface between air and water and between water and the sandy bed frame by frame. As shown in Figure 4, lab images were processed digitally for improvement by modifying the exposure, sharpening the image, and filtering noise. The bed profile and free water surface profile were automatically extracted in precise pixel coordinates. Then, distortion in the profiles of pixel coordinates was eliminated using a checkerboard algorithm. Finally, the image pixel coordinates of profiles without any distortion were translated to the actual position for the data regarding the beach profile and free surface elevation via interpolation using the four calibration points, which had been marked on the flume glass wall, as shown in Figure 5. The total station or auto level gauge and the wave instrument (wave gauge) were used to check the reliability and accuracy of the beach profile

and surface elevation data analyzed from the camera images [26,34]. This non-intrusive method using imaging technology showed promise for observation in the foreshore zone (inner surf zone and swash zone), where it is too shallow for the use and dense arrangement of traditional intrusive instrumentation.



**Figure 3.** Non-intrusive instrumentation for instantaneous measurements of the free water surface profile and beach transect.

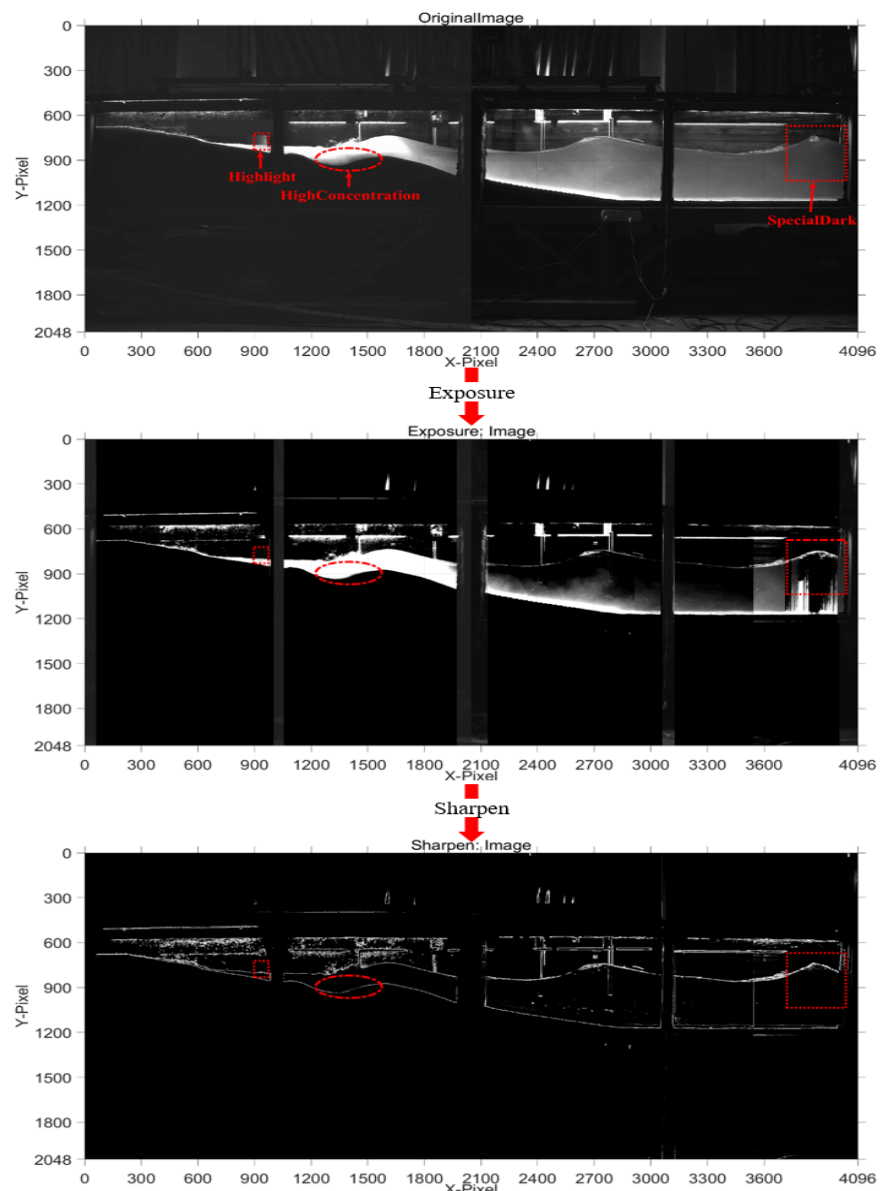


**Figure 4.** Numerical postprocessing of the exposure and sharpness of the original image.

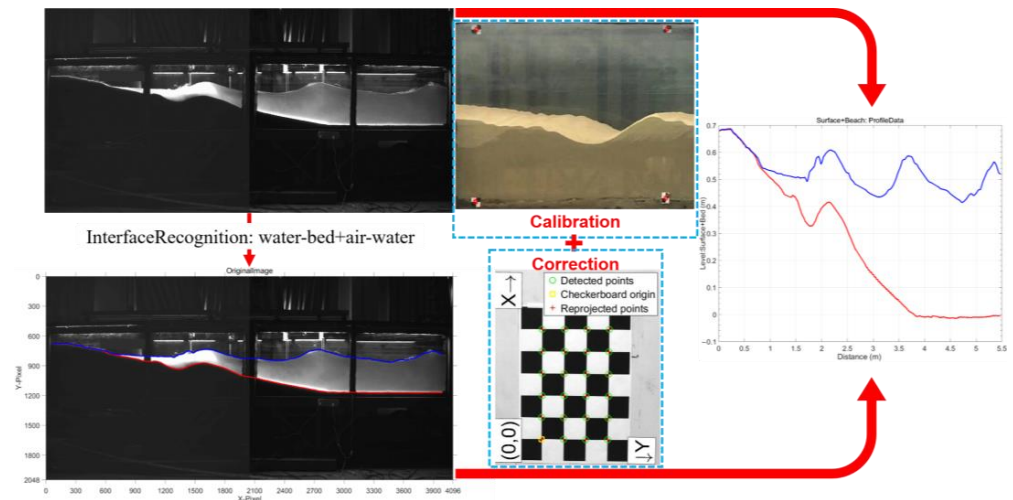


Figure 5. Step diagram for the experimental data measurement in the collection system.

#### 2.4. Definition of the Cross-Shore Beach Profile

The schematic diagram and the terminology used in this study to describe the beach profile are illustrated in Figure 6 [35–37]. The x coordinate is the horizontal coordinate from the wave paddle to the end of the beach profile, with the onshore direction being positive. The z coordinate is vertically directed in a positive direction from the flume bottom to the top of the flume window. Generally, the wave run-down limit should be the lowest vertical height of the swash zone; however, the rundown height is normally larger than the wave set-up on dissipative beaches but smaller than the wave set-up on reflective beaches [38]. According to on-site observations, the initial beach slope  $S = 1:10$  indicated an intermediate type between a dissipative and reflective beach, and the beach profile continually evolved with the staged changes in wave parameters. In this study, the still water level (SWL) and wave breaking point (*brp*) on the initial equilibrium profile of calm waves were regarded as the lowest boundary of the swash and surf zones, respectively. Thus, as shown in Figure 6, the cross-shore profile was defined as three regions: (1) the swash zone and dune *swz*, from the landward boundary to the SWL; (2) the surf zone *sfz*, from the SWL to the *brp*; and (3) the shoaling zone *shz*, which extended from the *brp* to the toe of the beach slope. Owing to the high resolution of the real-time beach profile and free surface elevation profile during storm simulation, the wave height transformation along the beach profile was analyzed, and the x coordinate of the largest wave height was the position of *brp*. The corresponding sediment transport rate  $Q(x)$  and net sediment volume change in the shoaling zone  $M_{shz}(t)$ , surf zone  $M_{sfz}(t)$ , and swash zone  $M_{swz}(t)$  could also be estimated using the real-time beach profile. As described by Wang et al. [26],  $M(t)$ , with  $m^2/s$  as the unit and positive stranding for accretion, was determined as follows:

$$M(t) = \sum_{x=a}^{x=b} (\partial z_b(t) dx) \tag{1}$$

where  $z_b$  is the bed elevation increment. Then, the net volume changes in the swash zone  $M_{swz}(t)$ , surf zone  $M_{sfz}(t)$ , shoaling zone  $M_{shz}(t)$ , and whole beach profile  $M_{all}(t)$  were calculated as follows:

$$M_{swz}(t) = \sum_{x=-\infty}^{x=SWL} (\partial z_b(t) dx) \tag{2}$$

$$M_{sfz}(t) = \sum_{x=SWL}^{x=brp} (\partial z_b(t) dx) \tag{3}$$

$$M_{shz}(t) = \sum_{x=brp}^{x=-\infty} (\partial z_b(t) dx) \tag{4}$$

$$M_{all}(t) = \sum_{x=-\infty}^{x=-\infty} (\partial z_b(t) dx) \tag{5}$$

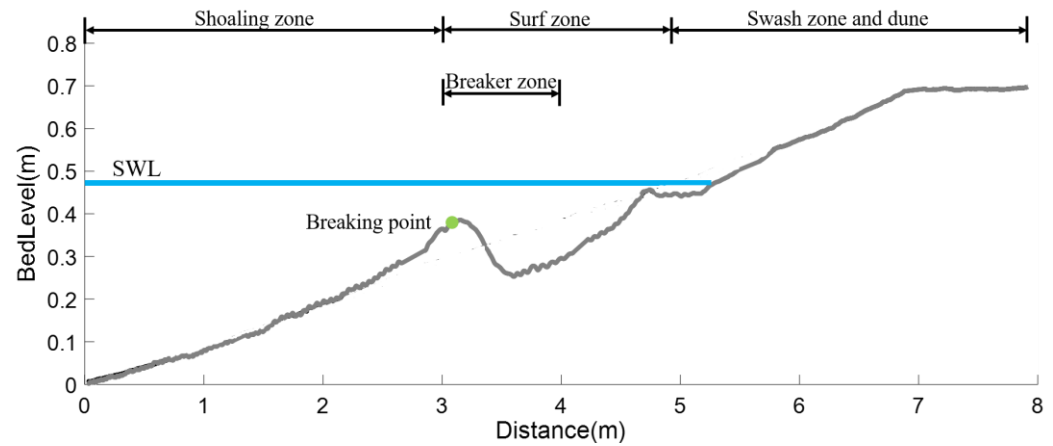


**Figure 6.** Schematic of beach profile showing different zones of a barred beach profile.

The high-resolution beach profile data allowed for the more reliable integration of net sediment transport  $Q(x)$  through the sediment volumetric conservation law [39]. The local cross-shore net sediment transport per unit width  $q_t(x_i)$  was calculated through Equation (6), and the landward boundary ( $Q(x = \infty) = 0$ ) was known for the integration of Equation (6).  $Q(x)$  (units  $m^2/s$ ,  $Q(x) > 0$ : onshore sediment transport) was provided by Equation (7):

$$q_t(x_i) = q_t(x_{i-1}) + \int_{x_{i-1}}^{x_i} \frac{\Delta z_b(x_i)}{\Delta t} dx \tag{6}$$

$$Q(x) = \Delta t \int_{\infty}^x q_t(x) dx \tag{7}$$

where  $\Delta z_b(x_i)$  is the change in bed elevation, and  $\Delta t$  is the time difference between the compared beach profiles. Given the integration of the beach profile with the shoaling zone, it was easy to produce calculation errors, mainly due to the impact of sand ripples. In addition to the calculation errors, the suspended sediment could also not be ignored because the real-time beach profile was collected during wave action, and the suspended sediment did not settle down, resulting in non-conservation. As it was mainly concentrated on beach morphology, this study took no account of the liquefaction of the sandy bed and its effects on porosity. For these reasons, the results had some problems with non-conservation. They were always slightly less than zero. It was difficult to return a value identical to zero by ignoring the influence of these parameters on the sediment flux in 1 min intervals.

As a wave propagates in the landward direction, the wave shape is typically characterized by a gradual peaking of the wave crest, flattening of the trough, and relative steepening of the face until breaking occurs, accompanied by a decrease in water depth as the wave undergoes shoaling. Understanding nearshore morphodynamics requires a profound knowledge of cross-shore hydrodynamics and their complex interaction with a mobile sandy bed. According to the high-resolution and cross-shore surface elevation data obtained using the image processing method, the cross-shore variation in wave skewness ( $Sk_\eta$ ) and wave asymmetry ( $Ay_\eta$ ) could be used to investigate the associated sediment transport. These parameters have been widely used for studying cross-shore sediment transport. Hence, the crest-to-trough asymmetry (wave skewness) and seaward-to-landward asymmetry of the free-surface elevation (wave asymmetry) are estimated as follows [40,41]:

$$Sk_\eta = \frac{\langle (\eta - \bar{\eta})^3 \rangle}{\langle (\eta - \bar{\eta})^2 \rangle^{3/2}} \tag{8}$$

$$Ay_\eta = \frac{\langle \mathcal{H}(\eta - \bar{\eta})^3 \rangle}{\langle (\eta - \bar{\eta})^2 \rangle^{3/2}} \tag{9}$$

where  $\eta$  is the free surface elevation,  $\bar{\eta}$  is the mean water level,  $\langle \rangle$  is the time-averaging operator, and  $\mathcal{H}$  is the imaginary part of the Hilbert transform. The change in wave shape during onshore propagation is considered to be an indicator of the response to wave nonlinearities along the beach profile because it is believed that the wave nonlinearities are proportional to the wave shape. Additionally, there are some other nonlinear wave transformation parameters that influence wave transmission over a cross-shore beach, such as the Iribarren number  $\zeta$ , Rocha number  $NP_0$ , [42] and Ursell number [43]. However, most of these parameters have a similar relationship with wave asymmetry parameters, and in contrast to the other nonlinear parameters, only  $NP_0$  is sensitive to differences in beach slope. There were slight differences in the range of changes in the other nonlinear parameters, but there was no difference in the rate of cross-shore changes in beach slope. Additionally, there was a clear linear positive correlation between  $NP_0$  and the linear wave velocity amplitude  $U$  in Wang et al. [27]. This means that  $NP_0$  could also be sensitive to changes in beach morphology during beach evolution and could be used to roughly estimate the change in cross-shore wave velocity. According to the linearized wave equation, the wave velocity amplitude  $U$  is determined as follows:

$$U = A\omega \frac{\cosh[k(z + d)]}{\sinh kd} = K_u A, K_u = \omega \frac{\cosh[k(z + d)]}{\sinh kd} \tag{10}$$

where  $A$  is the amplitude of free surface elevation,  $\omega$  is the wave angular frequency ( $\omega = 2\pi/T$ ),  $k$  is the wave number,  $d$  is the water depth, and  $z$  is the measurement gauge depth in the vertical direction. As mentioned in Rocha et al. [42], the  $NP_0$  was used for taking into account the beach slope by modifying the Ursell number:

$$NP_0 = \zeta(H/L)^2 \tag{11}$$

$\zeta$  is described as follows:

$$\zeta = \tan\beta / \sqrt{H/L} \tag{12}$$

where  $H$  is the local significant wave height,  $L$  is the wave length, and  $\tan\beta$  is the beach slope.

### 3. Results

Different from the monotonous evolution to equilibrium under monochromatic waves [44], beach profiles continually change with *brp* sea-landward migration during the sequence of wave height and water level change during a storm. Such frequent modifications caused the complexity of the present study. In the present study, changes in wave height and water levels were regarded as the main threat to coastal beaches in a storm event. The impact of a storm is directly manifested through changes in beach behavior, wave hydrodynamics, and associated sediment transport. To plan for and mitigate the damage caused by storms, shoreline and sandbar development and cross-shore sediment exchange associated with the transformation of cross-shore wave hydrodynamics can be used to investigate the disaster-causing factors of storm erosion.

#### 3.1. Morphological Response

The evolution of a beach profile due to storm action is a morphological process, in which the balance of a natural equilibrium profile or dynamically stable beach profile is damaged. Starting with the equilibrium profile after a 4 h period of calm waves ( $H = 0.1$  m,  $T = 1.5$  s,  $d = 0.46$  m), the morphological characteristics of beach evolution during a storm were evaluated by comparing each stage of beach profile evolution and the changes in beach behavior. The changes in the beach profile after each phase of the storm simulation

are shown in Figure 7. The beach profile data are plotted in Figure 7a,b, which present the corresponding image using a small camera aperture in the image processing method. In contrast to the small size of the sandbar and weak foreshore erosion in the initial equilibrium profile ( $t = 0$  min), after the rising phase, the intensification of the storm substantially modified the whole beach profile, with a larger-size sandbar that migrated seawards and more severe foreshore erosion in both the horizontal and vertical directions. Net erosion of the beach was observed from  $x = 3.8$  to  $6.3$  m. The shoreline retreated to  $x = 6.3$  m (original equilibrium shoreline  $x = 5.6$  m), and vertical erosion increased by about 5–10 cm, with the most serious vertical erosion occurring at the sandbar trough. The rest of the profile was covered with sand ripples. At the storm apex, foreshore erosion kept increasing, the shoreline further retreated to  $x = 6.6$  m, and the sandbar trough further eroded to  $y = 0.23$  m compared to  $y = 0.26$  m in the rising phase. The net erosion of the beach was observed from  $x = 4.0$  to  $4.9$  m and  $x = 5.2$  to  $6.6$  m, while evident accretion was observed from  $x = 4.9$  to  $5.2$  m. The accretion level was even higher than that of the initial equilibrium profile. This may mean that the erosion sediment from a shoreline retreat is deposited and filtered offshore, forming a sandbar that influences the foreshore. Such accretion under the higher-energy wave within the apex storm phase is discussed in Wang et al. [26]. The size of the sandbar only slightly increased and migrated landward from  $x = 3.6$  to  $3.7$  m. In the rest of the profile, mainly the shoaling zone, there was no change. Such a slight bed-level change could be attributed to the protection of a well-developed sandbar after the rising phase. The waning phase of the storm substantially reshaped the beach face, the foreshore zone was reconstructed, the sandbar trough was backfilled, and a berm was generated ( $x = 5.5$ – $6.2$  m). The shoreline no longer retreated, and the sandbar became smaller but migrated seawards. The foreshore zone tended to accrete, with net accretion observed from  $x = 4.0$  to  $4.8$  m and  $x = 5.5$  to  $6.2$  m. The shoaling zone also displayed accretion from  $x = 0$  to  $x = 3.5$  m, especially from  $x = 1.9$  to  $2.9$  m. Net erosion was observed as the sandbar diminished in size and migrated seawards from  $x = 4.0$  to  $3.5$  m.

Combining Figure 7a,b, starting with the equilibrium profile of the calm wave, the upper beachface sediment was generally carried out to the lower beach in each phase of the storm. As the wave height and water level increased, the shoreline kept retreating, and the sandbar tended to migrate offshore in the rising and apex phases compared with the original equilibrium profile. The sandbar switched forth slightly during the apex phase and grew by a few centimeters. A quite different trend was observed compared to the rising phase; however, the sandbar accreted slightly during the storm apex. The storm waning reconstructed the shore, and the sandbar advanced seaward from its initial position. In contrast to the other two phases of the storm, even though the foreshore zone evidently recovered during the waning phase, the shoaling zone was also subjected to accretion, and, therefore, there was almost no sediment transported from the deep offshore water to replenish the foreshore zone. The sandbar decreased in size and migrated seaward. The sediment scapped and was released from the sandbar deposited on the lower beach face, resulting in strong accretion in the shoaling zone. Therefore, the accretion in the shoaling zone in the waning phase occurred due to the evolution of the sandbar. Although the apex phase had the largest wave height and water level, the rising phase induced more severe erosion and resulted in more obvious changes to the beach morphology, as also reported by Wang et al. [26]. Additionally, the large change in the wave energy flux due to the changes in wave height, wave period, and water level was the main factor controlling the formation and migration of the sandbar, resulting in beach erosion and accretion before and after the *brp*. The changes in the wave parameters were the main reason for severe erosion during the storm, rather than the large waves.

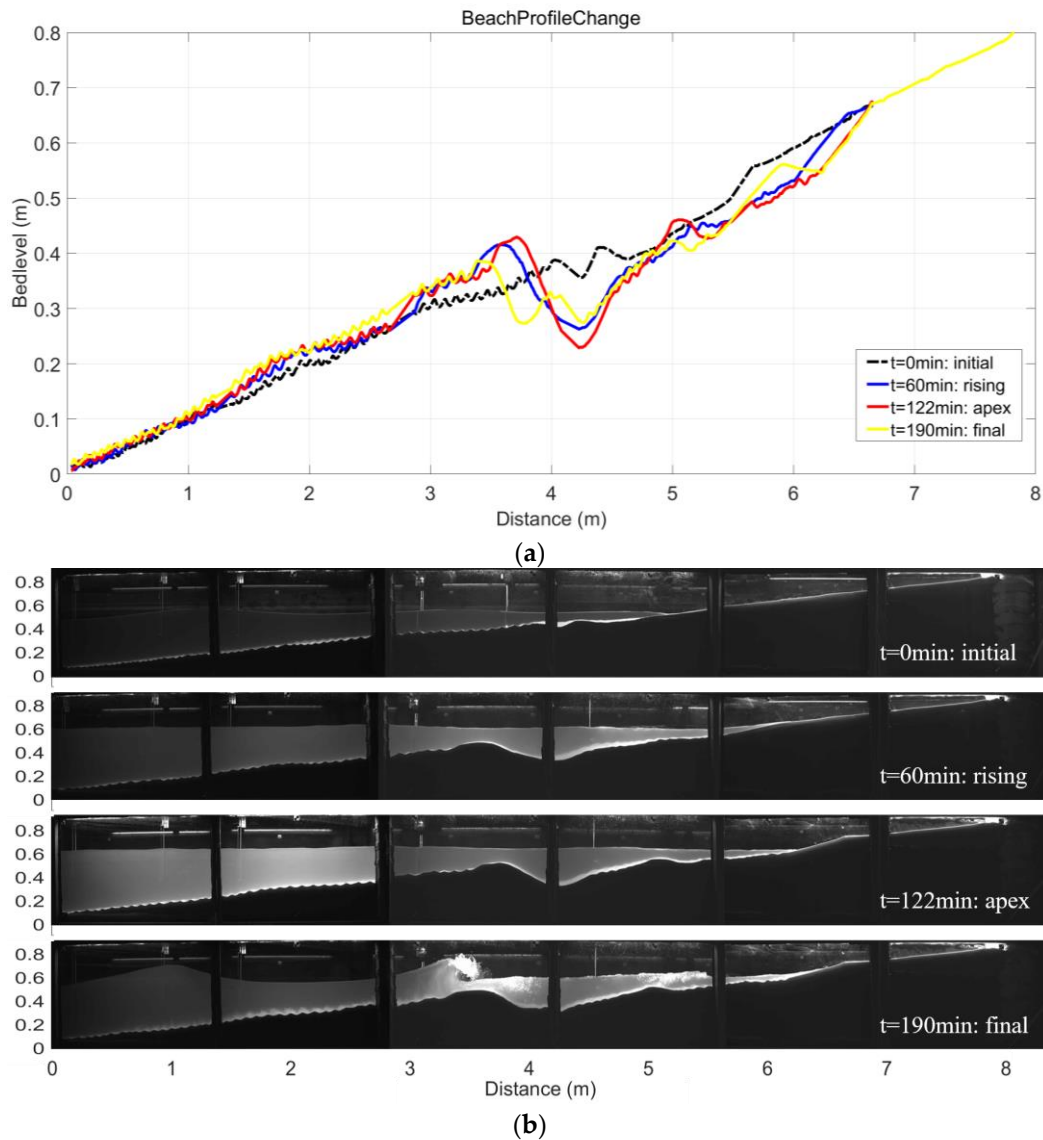


**Figure 7.** Beach profile changes after each phase of the storm. (a) Initial equilibrium beach profile after calm waves (dash-dotted black line), end of rising phase (solid blue line), end of apex phase (solid red line), and final waning phase (solid yellow line) beach profile during storm simulations. (b) The corresponding pictures of each storm phase.

To quantify the changes in beach behavior during the storm, Figure 8 shows the beach evolutionary processes, including the changes in the position and elevation of the sandbar, SWL, shoreline, and breaking waves. Figure 8a, b show a time series of the changes in the position and elevation of the breaking wave and sandbar crest during the storm simulation. The breaking wave was defined as the maximum wave height in the landward direction, and the sandbar crest was defined as the maximum positive bed-level change in relation to the initial equilibrium profile. The migration of the breaking wave was found to be related to the sandbar migration. They migrated offshore at approximately 1 m/h during the rising and waning phases of the storm, but there was slight onshore movement during the storm’s apex phase. The sandbar elevation and breaking wave height tended to increase during the rising phase, and both approached a maximum at the apex phase before decreasing almost to their original level after the waning phase. During the storm, the breaking wave maintained a close association with the motion of the sandbar, moving a nearly identical distance of approximately  $\Delta x \approx 0.3$  m, and the distance tended to increase during the waning phase. At the same time, the breaking wave height changed three times as fast

as the sandbar crest changed in the rising and waning phases. According to the position of the sandbar and the change in its elevation in Figure 8, as the wave height and water level changed during the storm, the sandbar migrated landward, serving as a filter for offshore large waves and promoting beach stability. However, regardless of these changes, the distance from the sandbar crest to the SWL always fluctuated around  $y = 0.11$  m during the storm. Additionally, the result of the calculation subtracting the wave breaking height from the SWL fluctuated around  $y = 0.32$  m, which may be because the difference between the SWL and incident wave height maintained a constant value ( $\Delta h \approx 0.36$  m) in each staged experiment of the storm simulation.

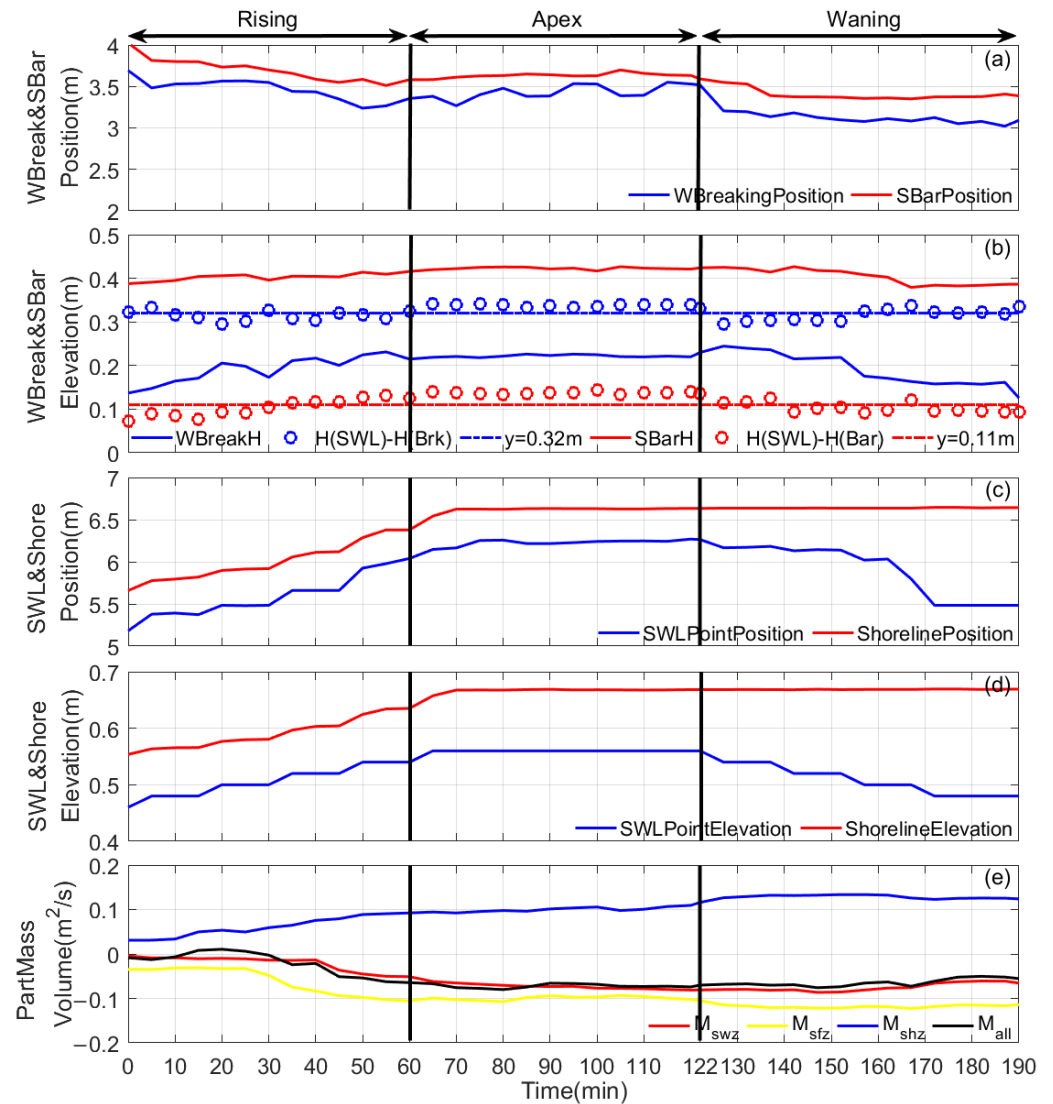


**Figure 8.** Temporal changes in (a) wave breaking and the bar crest position, (b) elevation and the elevation between the SWL and bar crest, (c) SWL and shoreline position, (d) elevation, and (e) variations in sediment volume in the cross-shore parts of the beach and total beach volume. Vertical solid lines delineate the three phases (rising, apex, waning) of the storm simulation.

The changes in the SWL and shoreline position and elevation are presented in Figure 8c,d. Their tendencies were clearly different from that of the sandbar, with the changes in the SWL always consistent with the changes in the shoreline in both the vertical and horizontal directions. The shoreline and SWL retreated significantly during the rising phase and to a lesser extent during the apex phase. During the rising and apex phases, the distance between the shoreline and SWL was almost invariant, with only a slight change

from the rising to the apex phases. This means that the slope of the swash zone was almost constant and in agreement with the slope of the swash zone in the equilibrium profile. Combined with the sandbar migration shown in Figure 8a,c, the distance between the sandbar, shoreline, and SWL tended to increase as the sandbar migrated offshore, and the shoreline and SWL retreated onshore during the rising phase. This extension in distance and the swash zone slope approaching the equilibrium slope likely played an important role in impeding further erosion and promoting beach stability. However, the distance was only slightly extended at the initial stage of the apex phase. In the waning phase, the SWL moved seaward, approaching the initial position, but it did not quite return to its initial position in both the vertical and horizontal directions. However, as the water level and wave height continued to decrease, the shoreline after the apex phase became increasingly difficult to impact, and the shoreline no longer changed during the storm waning phase.

The cross-shore sediment exchange can be explained by Figure 8e. The sediment mass in the shoaling zone increased almost continuously, in contrast to the surf zone, where sediment erosion was almost continuous. Rapid changes in sediment volume during the rising phase were characteristic of the considerable offshore sediment transport from the surf zone to the shoaling zone. In contrast, the cross-shore sediment transport in the apex phase became weaker in keeping with the slight changes in the sandbar, SWL, and shoreline. In addition to the surf zone, the swash zone was also continuously eroded, but the amplitude of the sediment volume fluctuations was always less than that of the surf zone, meaning that the surf zone was the main erosion region in the beach profile. Consistent with the earlier observations of Ruessink et al. [45], the sandbar formed primarily because of a decline in offshore-directed transport from the surf zone toward the shoaling zone, rather than the classic breakpoint hypothesis for sandbar generation, i.e., the convergence of onshore transport in the shoaling zone and offshore transport in the surf zone. Nevertheless, these exchanges diminished from the surf or swash zones to the shoaling zone during the waning phase, where the mass no longer changed, even though there was a slight adverse change in the shoaling and swash zones after  $t = 160$  min. The waning phase played some role in beach recovery: some of the sediment lost offshore was carried out from the shoaling zone to the swash zone. Finally, according to the total sediment volume fluctuations, i.e.,  $M_{all}$  in Figure 8e, even though the mass of sediment was constant during the storm simulation, there was continuous sediment loss in this closed system. These slight variations may be due to the apparent changes in sediment volume, i.e., changes in porosity (Grasso et al. [13]), or because the observed beach slope toe was not an absolute closure point, and the rising and apex phases then induced sediment loss.

### 3.2. Cross-Shore Wave Nonlinearity and Associated Sediment Transport

The cross-shore changes in the wave parameter sequence were the main driver of changes in beach morphology, and the variation in cross-shore sediment transport was directly related to local hydrodynamic parameters. Therefore, the following analysis is based on the changes in wave hydrodynamic parameters along the beach profile. The cross-shore wave nonlinear characteristics and mean wave velocity amplitude were represented by the wave asymmetry parameters ( $Sk_{\eta}$ ,  $Ay_{\eta}$ ) and  $NP_0$ , and their effects on sediment transport during each storm phase were evaluated.

Figure 9 summarizes the cross-shore transformation of wave skewness and wave asymmetry (top two lines) and the  $NP_0$  (third line) along the corresponding beach profile in the three phases of the storm simulation. The net sediment transport rate and changes in the beach profile are also shown. In the rising phase ( $H = 0.12\text{--}0.18$  m,  $T = 1.5$  s,  $d = 0.48\text{--}0.54$  m), the cross-shore nonlinear parameters displayed one obvious breaking zone extending from  $x = 3$  m, with the peak value of wave asymmetry and  $NP_0$  produced in the surf zone (Figure 9a,d,g). The changes in wave skewness and  $NP_0$  displayed similar features, with increases from the shoaling zone and a peak value approached after  $x = 3$  m, which then decreased in the foreshore zone (inner surf zone + swash zone). As a consequence, the  $NP_0$  almost followed the same trend, but the peak value tended to be measured onshore

(around  $x = 3.5$  m), and the decreasing stage was more rapid and smooth, with no irregular intersections between the different cross-shore data for different moments in time, as was observed for wave skewness  $Sk_\eta$ . In contrast to  $Sk_\eta$  and  $NP_0$ , wave asymmetry  $Ay_\eta$  presented a symmetrical trend with  $Sk_\eta$  to some extent, although it decreased in the shoaling zone and maintained a negative peak value from  $x = 3$  to 5 m in the surf zone. No temporal variation in  $Sk_\eta$  and  $Ay_\eta$  was evident. In contrast, the  $NP_0$  displayed an obvious temporal variation among the different stages, and the position of the peak value clearly moved among the different stages. It moved from  $x = 3.6$  m at  $t = 15$  min and  $t = 30$  min to  $x = 3.4$  m at  $t = 45$  min and  $t = 60$  min as the wave height and water level increased. The corresponding sandbar crest also clearly migrated, and the position of the peak value of the  $NP_0$  fell only slightly behind the sandbar crest (Figure 9m). The sandbar was the indicator of changes in the cross-shore nonlinear parameters because cross-shore wave transformation was directly related to wave breaking. Changes in sediment transport were considered in relation to the variations in  $Sk_\eta$ ,  $Ay_\eta$ , and the  $NP_0$ . The associated nonlinear-induced sediment transport  $Q$  was directed offshore with negative  $Q$  values (Figure 9j). As the wave height and water level increased, the sediment transport  $Q$  of the different stages also tended to increase. The final stage at  $t = 60$  min had the largest offshore sediment transport under the largest wave height and water level. In the seaward direction, the offshore sediment transport increased from the swash zone and approached a peak value in front of the sandbar, then decreased to zero at the end of the shoaling zone. Because there was no obvious temporal variation in  $Sk_\eta$  and  $Ay_\eta$  between the different stages, the changes in wave shape in the cross-shore nonlinear transform were approximated under the different wave heights and water levels during the rising phase. In contrast, for the  $NP_0$ , there were obvious differences in the amplitude between the different stages, and the position of the peak value was consistent with sandbar migration.

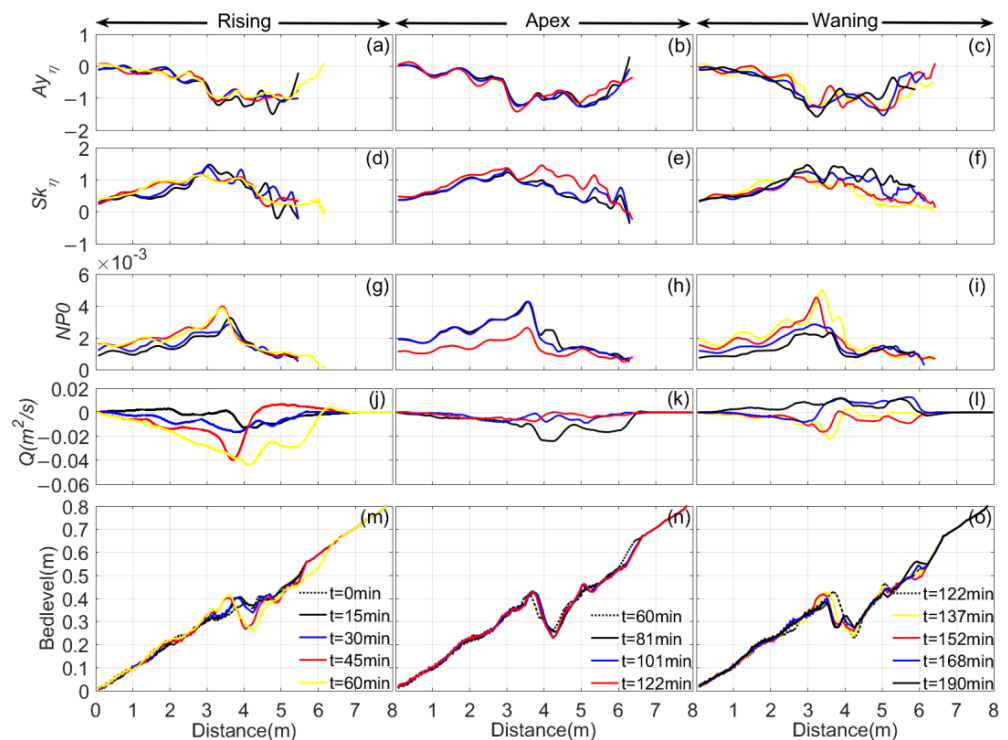


**Figure 9.** From top to bottom: changes in (a–c) cross-shore wave asymmetry  $Ay_\eta$ , (d–f) cross-shore wave skewness  $Sk_\eta$ , (g–i) Rocha number  $NP_0$ , (j–l) sediment transport rate  $Q$ , and (m–o) beach profile during each respective phase of the storm.

During the storm apex phase (constant  $H = 0.2$  m,  $T = 1.5$  s,  $d = 0.56$  m), the changes in wave asymmetry parameters were similar to those of the rising phase, with no irregular

cross-shore fluctuation. The temporal variations in wave skewness and wave asymmetry no longer intersected in the different stages under these constant wave parameters (Figure 9b,e,h). Overall, the cross-shore change in  $Sk_\eta$ ,  $Ay_\eta$ , and the  $NP_0$  followed the same trend as in the rising phase. The main difference from the rising stage was in the relationship between the different stages, especially for  $Sk_\eta$  and  $Ay_\eta$ , for which there were no irregular fluctuations between the different stages. The sandbar was also an indicator for distinguishing the location of the peak values of nonlinear parameters (seaward side of the sandbar) and peak offshore sediment transport (shoreward side of the sandbar), and the changes in the peak value were also associated with the position of the sandbar crest (Figure 9k,n). When considering the different stages, even though there was only a slight change in the beach profile without a change in the water level, the first two stages of the  $NP_0$  at  $t = 81$  min and  $t = 101$  min had a larger amplitude than that of the final stage  $t = 122$  min, especially in the shoaling zone and surf zone; these differences tended to decrease beyond the sandbar ( $x = 3.6\text{--}6$  m). The cross-shore tendencies of  $Sk_\eta$ ,  $Ay_\eta$ , and the  $NP_0$  were almost identical and clearly different from the cross-shore change in the final stage at  $t = 122$  min. Although there was an obvious change in the cross-shore amplitude of the  $NP_0$ , which differed from the rising phase, the position of the peak value did not change. From  $t = 60$  min to 81 min, there was a slight migration and development of the sandbar, but afterward, the sandbar displayed minimal migration and growth. Although the amplitude of the nonlinear parameters almost agreed with the amplitude in the rising phase under the largest wave height and water level, cross-shore sediment transport was generally lower than during the rising phase. Consistent with sandbar migration from  $t = 60$  min to 81 min, the initial stage  $Q$  ( $t = 81$  min) had the greatest level of offshore sediment transport, after which the sediment transport in the other two stages decreased substantially to a very low level. In the second stage ( $t = 101$  min), although  $Sk_\eta$ ,  $Ay_\eta$ , and the  $NP_0$  still displayed the same cross-shore changes as in the first stage, the weak offshore sediment transport was concentrated in the inner surf zone and swash zone, with deeper sandbar trough scouring. Only in the third stage ( $t = 122$  min) was there an obvious difference between the cross-shore nonlinear parameters, with a smaller amplitude in the  $NP_0$  and slightly larger amplitudes of  $Sk_\eta$  and  $Ay_\eta$ . The weak offshore sediment transport was concentrated in the surf zone, with a slight seaward modification of the sandbar on the shoreward side.

During the waning phase, the changes in wave asymmetry were similar to those in the rising phase in terms of both the cross-shore tendency and the relationship between the different stages. The peak values of the nonlinear parameters and offshore sediment transport occurred on the seaward and landward sides of the sandbar, respectively. The cross-shore amplitude of  $Ay_\eta$  and the  $NP_0$  at  $t = 137$  min and 152 min tended to increase compared with the symmetric stages of the rising phase (Figure 9c,f,i,l,o). The amplitude of  $Ay_\eta$  only increased slightly, while the two stages of the  $NP_0$  ( $t = 137$  min and 152 min) were clearly larger than in the two symmetric stages of the rising phase. Additionally, the cross-shore fluctuation in  $Sk_\eta$  and  $Ay_\eta$  after the peak point tended to be magnified, and the rate of decrease in  $Sk_\eta$  slowed down at  $t = 168$  min and 190 min. In contrast to the evolution of the foreshore morphology during the rising phase, the changes in foreshore morphology between the different stages were more prominent in the waning stage; therefore, the amplification of cross-shore fluctuation was likely related to a significant foreshore evolution. However, under the changes in wave asymmetry and larger amplitude of nonlinear parameters, the degree of change in the beach profile and sediment transport was smaller than that observed during the rising phase, and, therefore, the beach profile and wave parameter change sequence likely also played some role in cross-shore sediment transport. At the larger wave stage at  $t = 168$  min and  $t = 190$  min, sediment transport reversed compared with the symmetric stage of the rising phase, and onshore sediment transport occurred in the foreshore zone concurrently with the diminishing of the sandbar and its seaward migration. As a consequence, a beach berm was generated in the swash zone (around  $x = 6$  m).

As shown in the comparison of the three different storm phases, variations in the wave parameters induced changes in the cross-shore evolution of the nonlinear parameters. The stage with the smallest wave height and water level always had a slightly larger amplitude of wave asymmetry parameters. In contrast, a larger wave height and water level was associated with a larger amplitude cross-shore change in the  $NP_0$ . The symmetry stage had the same wave parameters, but the performance of the nonlinear parameters differed under the different initial beach profiles and sequences of wave parameter changes. Although they had almost the same initial value and similar relationships between the different stages, the performance after the peak value and amplitude of the changes were clearly different. The perturbation of  $Sk_{\eta}$  and  $Ay_{\eta}$  after the peak value tended to be magnified, and the cross-shore change amplitude tended to increase slightly in both the wave asymmetry parameter and the  $NP_0$ , especially for the  $NP_0$ . The changes in the amplitude of the  $NP_0$  at  $t = 137$  min and  $t = 152$  min were larger than in the corresponding stage in the rising phase, and they were even slightly larger than in the first two stages of the apex phase, which had the largest wave height and water level. In addition to the changes in wave parameters, the influence of the changes in the beach profile was also significant in the simulation.

In contrast to the rising and waning phases, although the largest wave height and water level was held for the same duration (1 h) in the apex phase, changes in the beach profile were not apparent without associated changes in the sandbar and foreshore morphology, which corresponded with a stable location of the peak value and a smaller amplitude of the cross-shore nonlinear parameters. This could be attributed to the larger size of the sandbar after the rising phase filtering the large waves. The sandbar and wave parameter sequence will, therefore, play an important role in estimating storm hazard. As mentioned above, the evident migration and evolution of the sandbar was always accompanied with the cross-shore motion of the  $NP_0$  and the maximum velocity amplitude. Combined with the temporal and spatial variation of the  $NP_0$  and sediment transport rate  $Q$  in Figure 10, during changes in the wave parameter sequence, the significant motion of the peak value of the  $NP_0$  (as pointed out by the yellow arrow) is always associated with more intense sediment transport, and the maximum offshore sediment of the rising phase and onshore sediment of the waning phase also occurred around those times. While the sediment transport of the apex phase was significantly weaker than the other two phases, it corresponded to the relatively stable position of the peak value of the  $NP_0$ .

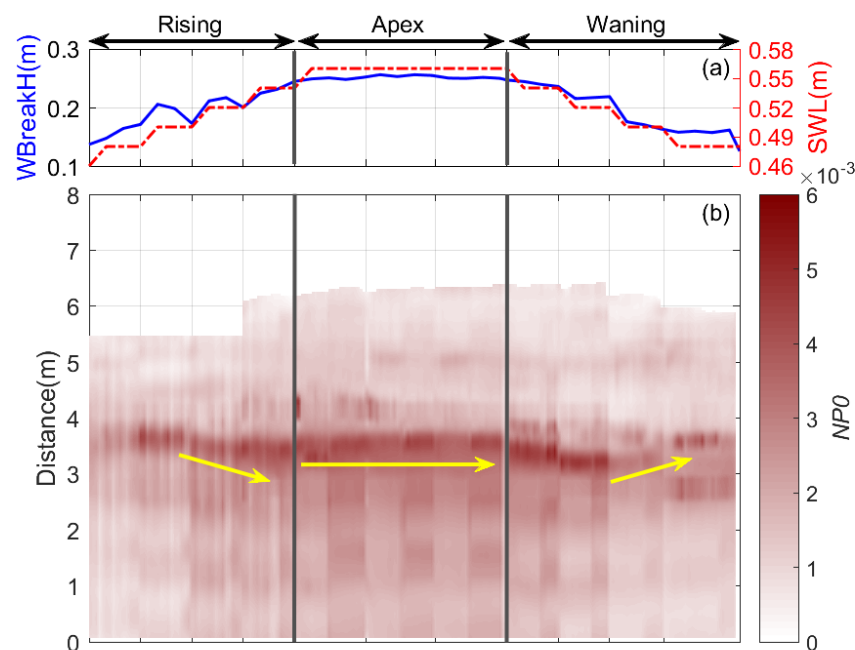
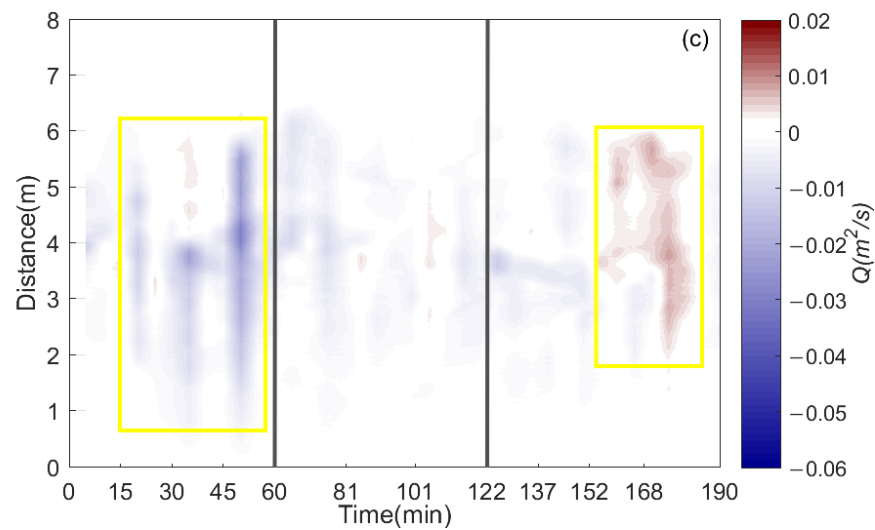


Figure 10. Cont.



**Figure 10.** From top to bottom: (a) breaking wave height and SWL, (b) the time variation in cross-shore  $NP_0$ , and (c) the time variation in the cross-shore sediment transport rate  $Q$  during the storm. In the  $NP_0$  colormap, the color of  $NP_0$  changes from white to red as the values increase. In the sediment transport rate ( $Q$ ) colormap, blue represents offshore sediment transport and red represents onshore sediment transport.

#### 4. Discussion

##### 4.1. Image Processing Analysis

It has been demonstrated that flume experiments can serve as an alternative to field measurements and numerical modeling for studying the response of beaches to different wave climates. Although there are limitations in the experimental scale, a smaller-scale size as that of the flume in this study can also be regarded as an alternative approach to describing the laws of nature, because they behave in qualitatively similar ways to prototype beaches and form the same characteristic features [46,47]. Furthermore, the limited availability of data always makes it difficult to distinguish the contributions of longshore and cross-shore sediment transport due to the inherent complexity of natural beaches [48], whereas a flume experiment can focus on cross-shore sediment transport. Image processing appears to provide a useful tool for the non-intrusive measurement of real-time beach morphodynamics in a wave flume, and because wave data and beach profile data are obtained from the same camera image, the wave and beach profile data are guaranteed to be completely synchronized. For obtaining clear air–water and water–bed interfaces, in a laboratory-based wave flume, a window shade can be erected to exclude sunlight and avoid the influence of sunlight on image intensities over time or the influence of changes in the weather. This improvement was first suggested by Palmsten and Holman [14], but in the present study, it was enhanced by the use of sunlight lamps above the wave flume. The use of sunlight lamps together with a window shade not only ensured a constant image intensity but also enabled light to pass through water with a high concentration of suspended sediment to obtain a clear water–bed interface. Additionally, a postprocessing program was also developed to further improve the accuracy of the air–water and water–bed interfaces through a numerical method of modifying exposure, sharpening images, and filtering wavelets. However, there were still some problems in catching the free water surface after wave breaking, and improvements need to be made. The rapid downward spreading of breaking-induced turbulence and the large number of air bubbles entrained during wave breaking induced the overexposure of the image, and, therefore, there were still some errors in catching the free water surface of the inner surf zone. A bubble image velocimetry (BIV) system with a microfocus and lower camera aperture may be required to avoid the overexposure of images in future research. Alternatively, multiple cameras with different exposure settings could be used to capture

the same area simultaneously. This is because, to some extent, the BIV system always needs to be provided with sufficient light exposure to capture the shadows of the bubbles, which can then be used to determine the velocity of the bubble area. It may still not prevent image overexposure.

#### 4.2. Storm Erosion Analysis

The physical processes involved in the evolution of sandy beaches under storm conditions were investigated. In the storm simulations, the staged changes in wave height and water level had distinct effects on beach morphodynamics. The rising phase led to rapid beachface erosion with a high offshore sediment transport rate, eroding the foreshore zone and enabling the sandbar to grow and migrate seaward [26]. The apex phase had a weaker cross-shore sediment transport than the rising phase but led to further shoreline retreat and slight growth of the sandbar. The region where the largest effect was observed was the swash zone, with the highest wave runup occurring under the largest wave height and water level. In contrast to the rising and apex phases, the waning phase corresponded to weak offshore sediment transport at the initial stage, which then shifted to onshore sediment transport and beachface accretion. However, onshore sediment transport was mainly from the original larger sandbar. In a medium-scale wave flume, most wave conditions produce small waves with a short wave period due to the limitation of the flume length. These waves are not able to transport the sediment in the shoaling zone onshore. This explains the monotonous relationship between cross-shore sediment exchange–foreshore erosion and offshore accretion in most stages of the storm simulation. The deterioration of the sandbar made a larger contribution to the onshore sediment transport of the waning phase than the sediment volume in the negative shoaling zone.

The differing performance between the three storm phases, especially between the rising phase and waning phase, implied that changes in the wave parameter sequencing of different storm phases were important for determining the behavior and rate of change of beach morphology during storms. During the storm phases, the wave asymmetry parameters  $Sk_\eta$  and  $Ay_\eta$  varied with the intensification of disturbance in the foreshore zone during the different stages. This is supposed to lead to frequent changes in wave nonlinearity across the foreshore zone, indicating an extremely turbulent environment, where wave action could mobilize more bed sediment. Compared with  $Sk_\eta$  and  $Ay_\eta$ , the  $NP_0$  could better represent the changes in wave parameters, and a larger wave height and water level were associated with a larger amplitude in the cross-shore change of the  $NP_0$ , accompanied by a larger amplitude of the cross-shore wave velocity. Both an increase in suspended sediment and a larger amplitude in cross-shore wave velocity could promote the offshore transport of foreshore sediment. However, the amplitude of the cross-shore changes in the  $NP_0$  could still decrease when the wave parameters were constant as the beach approached an equilibrium state at the third stage of the apex phase. This could be attributed to the changes in the wave parameter sequence. In other words, the gradient of wave parameter sequence change in the apex phase was zero, the beach approached an equilibrium state under constant wave forcing over time, and, therefore, the amplitude of the cross-shore wave velocity tended to decrease as the beach became more and more stable. In contrast to the constant wave parameter sequence in the apex phase, the gradient of wave parameter sequence change in the other storm phases was not zero, and the beach was continually modified together with a sea–landward migration of the sandbar. This further illustrates that the sequences of both the wave parameters and their sequence change gradient should play some role in cross-shore sediment transport during a storm.

The different sequences of wave height and water level directly affect variations in cross-shore hydrodynamics which then impact bottom sediment stir-up, and they were mainly reflected in the sea–landward migration of the sandbar in the process of beach morphology. The beach morphology after the previous stage, such as the presence of a relic sandbar, which could also influence the cross-shore sediment transport in the present stage, resulted in increasingly more complex sediment transport as the wave parameters

changed. The influence of the relic sandbar on sediment transport has been reported as a morphological hysteresis in the evolution of beach profiles [20]. Sandbar development will, therefore, also play an important role in determining the processes involved in storm erosion. In Larson et al. [48], a regression relationship was derived relating the non-dimensional equilibrium bar volume  $V_{bar}$  to the quantities  $H_0/\omega T$  and  $H_0/L_0$  as follows:

$$\frac{V_{bar}}{L_0^2} = 0.028 \left( \frac{H_0}{\omega T} \right)^{1.32} \left( \frac{H_0}{L_0} \right)^{1.05} \quad (13)$$

$$V_{bar} = 0.028 \left( \frac{H_0}{\omega T} \right)^{1.32} (H_0)^{1.05} (L_0)^{0.95} \quad (14)$$

Equation (14) explains the relationship between changes in the sandbar and wave parameters, in which  $H_0$  and  $L_0$  are the wave height and wave length in deep water, respectively;  $T$  is the wave period; and  $\omega$  is the sediment settling velocity. In the present experiment, although the beach did not have sufficient time to approach the corresponding equilibrium status with a well-developed sandbar for each wave parameter, the sandbar migration and development could still reflect the tendency of a beach to approach the corresponding equilibrium status. The sandbar also followed the same pattern in terms of both crest height and x coordinate (as shown in Section 3.1) as an efficient response to sandbar evolution and changes in wave parameters at different stages during a storm. The efficient response also agreed with the observations in the storm condition of a slowly varying wave height [34]. Under the same sand and a constant wave period, the sandbar volume  $V_{bar}$  should be positively related to wave height and water level. In keeping with the study by Ruessink et al. [45], the sandbar was generated primarily because of a decline in offshore-directed transport from surf erosion toward the shoaling zone rather than the convergence of onshore transport in the shoaling zone and offshore transport in the surf zone. The larger wave height and water level should be consistent with a larger sandbar, which indicates a more serious surf zone erosion.

The beach evolved toward equilibrium for each wave condition. Because there was an efficient response between sandbar evolution and the changes in wave parameters, the sandbar had been well developed in the initial stage. The largest positive gradient of wave parameter sequence change during the rising phase resulted in an evident increase in the size of the sandbar and the aggravation of surf zone erosion. Additionally, the cross-shore peak value of the wave nonlinear parameter occurred near the seaward side of the sandbar, leading to peak offshore sediment transport near the sandbar. The peak value of the nonlinear parameters was always consistent with the largest offshore sediment transport rate. As the indicator for cross-shore peak wave nonlinearity and offshore sediment transport, the evident migration of the sandbar indicated a more frequent motion of strong nonlinearity, high wave velocity, and severe offshore sediment transport, increasing the instability of the beach. In contrast to the rising phase, the zero gradient of changes in the wave parameter sequence should be in line with the slight change in sandbar volume in the apex phase, and the beach should approach equilibrium as time passes. The rate of change of beach morphology in each stage during the apex phase varied under the same wave conditions but was different in the initial beach profile (different sequencing). Although the wave parameters were the largest during the apex phase, the cumulative effect was not constant but decreased as the beach stabilized. Thus, the rising phase induced a larger amount of foreshore sediment erosion. Contrary to the rising phase, the waning phase had the largest negative gradient of change in the wave parameter sequence, which resulted in a more extensive decrease in the sandbar volume. The sediment scapped from the sandbar could contribute to onshore sediment transport. Therefore, similar to the description in Eichentopf et al. [19], the same wave condition could still result in either beach erosion or recovery, depending on whether the beach is in a recovered or eroded condition compared to the equilibrium beach configuration for these specific wave conditions. This also means

a change in the nonlinear tendency or characteristic of cross-shore waves rather than their value changing range in the cycle sequence.

## 5. Conclusions

Laboratory experiments were conducted to investigate the influence of changes in both variable wave height and water level on the evolution of a sandy beach profile during a simulated storm. The simulation of a schematic storm sequence included three different phases (rising, apex, and waning) and was conducted through the staged simulation of wave height and water level in a 2D wave flume. An innovative non-intrusive data collection system using a side-looking camera was successfully used to collect high-resolution and synchronous data regarding the free surface water elevation of waves and bed-level changes. The system was non-intrusive, without causing any disturbances to wave motions and the movable bed of sediment. It will hopefully solve measurement problems in nearshore environments. The synthesis of the present work shows that there was monotonous cross-shore sediment exchange from foreshore erosion to shoaling zone accretion in most stages of the storm simulation. The surf zone was the main zone supplying the sediment for the modification of beach morphology, especially sandbar generation, and swash zone erosion directly determined shoreline motion. The gradient of change in the wave parameter sequence was the reason for varying performance during the three storm phases. The rising phase, with the largest gradient of wave parameter sequence change, induced more severe and rapid beachface erosion instead of the apex phase, even though the apex phase was conducted using the peak values for the wave parameters for its entire duration. During the apex phase, the effects were mainly represented by further shoreline retreat as swash zone erosion became more significant under the higher runup. The offshore sediment transport became onshore transport due to the deterioration of the original large sandbar under the decreasing wave parameter sequence in the waning phase. The potential risk for beachface erosion during the storm was not completely dependent on larger wave parameters, but the larger gradient of the wave parameter sequence change was the main factor responsible for more severe storm erosion. It induced an increase in sandbar size that was accompanied by the cross-shore motion of maximum velocity amplitude and a more violent disturbance due to wave nonlinearity and increased surf zone erosion. Both of these factors increased real-time beach instability, leading to more severe erosion. In the future, coastal managers could typically invoke and potentially forecast the erosion potential prior to an oncoming storm given the gradient of changes in the wave parameter sequence during a storm.

**Author Contributions:** Methodology, J.W. and B.Y.; Software, J.W., B.Y. and Z.W. (Zhenlu Wang); Formal analysis, J.W.; Investigation, J.W.; Resources, B.L., Z.-J.Y. and Z.W. (Zhaowei Wang); Data curation, J.W., B.Y. and Z.W. (Zhenlu Wang); Writing—original draft, J.W.; Writing—review & editing, B.Y., B.L. and Z.-J.Y.; Supervision, B.L. and Z.-J.Y.; Project administration, B.L.; Funding acquisition, B.L., Z.-J.Y., Z.W. (Zhenlu Wang) and Z.W. (Zhaowei Wang). All authors have read and agreed to the published version of the manuscript.

**Funding:** This research was funded by the National Basic Research Program of China (Grant No. 2023YFC3007900), the National Science Fund of China (Grant Nos. U1906231, 52301345, and 52101338) and the China Postdoctoral Science Foundation (Grant Nos. 2023M733350).

**Institutional Review Board Statement:** Not applicable.

**Informed Consent Statement:** Not applicable.

**Data Availability Statement:** The data that support the findings of this study are available from the corresponding author upon reasonable request.

**Conflicts of Interest:** The authors declare that they have no known competing financial interests or personal relationships that could have appeared to influence the work reported in this paper.

## References

- Elgar, S.; Guza, R.T. Observations of bispectra of shoaling surface gravity waves. *J. Fluid Mech.* **1985**, *161*, 425–448. [[CrossRef](#)]
- King, D.B. Studies in Oscillatory Bed-Load Sediment Transport. Ph.D. Thesis, University of California, San Diego, CA, USA, 1991.
- Doering, J.C.; Bowen, A.J. Parameterization of orbital velocity asymmetries of shoaling and breaking waves using bispectral analysis. *Coast. Eng.* **1995**, *26*, 15–33. [[CrossRef](#)]
- Austin, M.; Masselink, G.; O'Hare, T.; Russell, P. Onshore sediment transport on a sandy beach under varied wave conditions: Flow velocity skewness, wave asymmetry or bed ventilation. *Mar. Geol.* **2009**, *259*, 86–101. [[CrossRef](#)]
- You, Z.J.; Nielsen, P. Extreme coastal waves, ocean surges and wave runup. In *Coastal Hazard Book*; Charles, W.F., Ed.; Coastal Research Library 6; Springer: Berlin, Germany, 2013.
- Karunarathna, H.; Pender, D.; Ranasinghe, R.; Short, A.D.; Reeve, D.E. The effects of storm clustering on beach profile variability. *Mar. Geol.* **2014**, *348*, 103–112. [[CrossRef](#)]
- Spencer, T.; Brooks, S.; Evans, B.; Tempest, J.A.; Moller, I. Southern North Sea storm surge event of 5 December 2013: Water levels, waves and coastal impacts. *Earth-Sci. Rev.* **2015**, *146*, 120–145. [[CrossRef](#)]
- You, Z.J.; Laine, R.; Wiece, D.; Hanslow, D.; Baldock, T. Field measurements of beach-dune dynamic profiles and grain-size distributions to assess coastal erosion along NSW coast of Australia. In Proceedings of the 34th Conference on Coastal Engineering, Seoul, Republic of Korea, 15–20 June 2014.
- Richard, S.; Guza, R.T.; William, O.R.; Steve, E. Rapid erosion of a small southern California beach fill. *Coast. Eng.* **2005**, *52*, 151–158.
- Donnelly, C.; Kraus, N.C.; Larson, M. State of knowledge on measurement and modeling of coastal overwash. *J. Coast. Res.* **2006**, *22*, 965–991. [[CrossRef](#)]
- Masselink, G.; Castelle, B.; Scott, T.; Dodet, G.; Suanez, S.; Jackson, D.; Floc'h, F. Extreme wave activity during 2013/2014 winter and morphological impacts along the Atlantic coast of Europe. *Geophys. Res. Lett.* **2016**, *43*, 2135–2143. [[CrossRef](#)]
- Harley, M.D.; Turner, I.L.; Kinsela, M.A.; Middleton, J.H.; Mumford, P.J.; Splinter, K.D.; Phillips, M.S.; Simmons, J.A.; Hanslow, D.J.; Short, A.D. Extreme coastal erosion enhanced by anomalous extratropical storm wave direction. *Sci. Rep.* **2017**, *7*, 6033. [[CrossRef](#)]
- Grasso, F.; Michallet, H.; Barthelemy, E. Experimental simulation of shoreface nourishments under storm events: A morphological, hydrodynamic, and sediment grain size analysis. *Coast. Eng.* **2011**, *58*, 184–193. [[CrossRef](#)]
- Palmsten, M.L.; Holman, R.A. Laboratory investigation of dune erosion using stereo video. *Coast. Eng.* **2012**, *60*, 123–135. [[CrossRef](#)]
- Aagaard, T.; Hughes, M.G.; Baldock, T.; Greenwood, B.; Kroon, A.; Power, H. Sediment transport processes and morphodynamics on a reflective beach under storm and non-storm conditions. *Mar. Geol.* **2012**, *326*, 154–165. [[CrossRef](#)]
- Larsen, B.E.; van der A, D.A.; Carstensen, R.; Carstensen, S.; Fuhrman, D.R. Experimental investigation on the effects of shoreface nourishment placement and timing on long-term cross-shore profile development. *Coast. Eng.* **2023**, *180*, 104258. [[CrossRef](#)]
- Ojeda, E.; Guillén, J. Monitoring beach nourishment based on detailed observations with video measurements. *J. Coast. Res.* **2004**, *SI48*, 100–106.
- Ojeda, E.; Ruessink, B.; Guillén, J. Morphodynamic response of a two-barred beach to a shoreface nourishment. *Coast. Eng.* **2008**, *55*, 1185–1196. [[CrossRef](#)]
- Eichentopf, S.; Der Zanden, J.V.; C'aceres, I.; Baldock, T.E.; Karunarathna, H.; Alsina, J.M. Beach profile evolution under storm sequence forcing in large-scale experiments. *Geophys. Res. Abstr.* **2019**, *21*, EGU2019-10417.
- Baldock, T.E.; Birrien, F.; Atkinson, A.L.; Shimamoto, T.; Wu, S.; Callaghan, D.P.; Nielsen, P. Morphological hysteresis in the evolution of beach profiles under sequences of wave climates-Part 1; observations. *Coast. Eng.* **2017**, *128*, 92–105. [[CrossRef](#)]
- Polidoro, A.; Pullen, T.; Eade, J.; Mason, T.; Blanco, B.; Wyncoll, D. Gravel beach profile response allowing for bimodal sea states. *Proc. Inst. Civ. Eng.* **2018**, *171*, 145–166. [[CrossRef](#)]
- Rosati, J.; Dean, R.; Walton, T. The Modified Bruun rule extended for landward transport. *Mar. Geol.* **2013**, *340*, 71–81. [[CrossRef](#)]
- Atkinson, A.L.; Baldock, T.E.; Birrien, F.; Callaghan, D.P.; Nielsen, P.; Beuzen, T.; Ranasinghe, R. Laboratory investigation of the Bruun Rule and beach response to sea level rise. *Coast. Eng.* **2018**, *136*, 183–202. [[CrossRef](#)]
- Atkinson, A.L.; Baldock, T.E. Laboratory investigation of nourishment options to mitigate sea level rise induced erosion. *Coast. Eng.* **2020**, *161*, 103769. [[CrossRef](#)]
- Beuzen, T.; Turner, I.L.; Blenkinsopp, C.E.; Atkinson, A.; Flocard, F.; Baldock, T.E. Physical model study of beach profile evolution by sea level rise in the presence of seawalls. *Coast. Eng.* **2018**, *136*, 172–182. [[CrossRef](#)]
- Wang, J.; You, Z.J.; Liang, B.C.; Wang, Z.W.; Yang, B. The physical processes of sandy beach evolution under storm and non-storm wave conditions simulated in wave flume. *Mar. Geol.* **2023**, *462*, 107065. [[CrossRef](#)]
- Wang, J.; You, Z.J.; Liang, B.C.; Du, J.F.; Yang, B. Non-Intrusive Measurements of wave non-linearity over movable bed of sediment with different beach slopes. *Phys. Fluids* **2024**, *36*, 017115. [[CrossRef](#)]
- Hughes, M.G.; Cowell, P.J. Adjustment of reflective beaches to waves. *J. Coast. Res.* **1987**, *3*, 153–167.
- Nielsen, P. Field-measurements of time-averaged suspended sediment concentrations under waves. *Coast. Eng.* **1984**, *8*, 51–72. [[CrossRef](#)]
- Ting, F.C.K.; Kirby, J.T. Observation of Undertow and Turbulence in a Laboratory Surf Zone. *Coast. Eng.* **1994**, *24*, 51–80. [[CrossRef](#)]

31. Aagaard, T.; Jensen, S.G. Sediment concentration and vertical mixing under breaking waves. *Mar. Geol.* **2013**, *336*, 146–159. [[CrossRef](#)]
32. van Der Zanden, J.; van der A, D.A.; Hurther, D.; Cáceres, I.; O'donoghue, T.; Ribberink, J.S. Suspended sediment transport around a large-scale laboratory breaker bar. *Coast. Eng.* **2017**, *125*, 51–69. [[CrossRef](#)]
33. Anfuso, G. Sediment-activation depth values for gentle and steep beaches. *Mar. Geol.* **2005**, *220*, 101–112. [[CrossRef](#)]
34. Wang, J.; You, Z.J.; Liang, B.C. Laboratory investigation of coastal beach erosion processes under storm waves of slowly varying height. *Mar. Geol.* **2020**, *430*, 106321. [[CrossRef](#)]
35. Elfrink, B.; Baldock, T.E. Hydrodynamics and sediment transport in the swash zone: A review and perspectives. *Coast. Eng.* **2002**, *45*, 149–167. [[CrossRef](#)]
36. Bakhtyar, R.; Barry, D.A.; Li, L.; Jeng, D.S.; Yeganeh-Bakhtiary, A. Modeling sediment transport in the swash zone: A review. *Ocean Eng.* **2009**, *36*, 767–783. [[CrossRef](#)]
37. Chardon-Maldonado, P.; Pintado-Patino, J.C.; Puleo, J.A. Advances in swash-zone research: Small-scale hydrodynamic and sediment transport processes. *Coast. Eng.* **2016**, *115*, 8–25. [[CrossRef](#)]
38. Gourlaym, R. Wave set-up, wave run-up and beach water table: Interaction between surf zone hydraulics and groundwater hydraulics. *Coast. Eng.* **1992**, *17*, 93–144. [[CrossRef](#)]
39. Baldock, T.E.; Manoonvoravong, P.; Pham, K.S. Sediment transport and beach morphodynamics induced by free long waves, bound long waves and wave groups. *Coast. Eng.* **2010**, *57*, 898–916. [[CrossRef](#)]
40. Elgar, S.; Guza, R.T.; Freilich, M.H. Eulerian measurements of horizontal accelerations in shoaling gravity waves. *J. Geophys. Res.* **1988**, *93*, 9261–9269. [[CrossRef](#)]
41. Nielsen, P. Sheet flow sediment transport under waves with acceleration skewness and boundary layer streaming. *Coast. Eng.* **2006**, *53*, 749–758. [[CrossRef](#)]
42. Rocha, M.; Michallet, H.; Silva, P.A. Improving the parameterization of wave nonlinearities—The importance of wave steepness, spectral bandwidth and beach slope. *Coast. Eng.* **2017**, *121*, 77–89. [[CrossRef](#)]
43. Ruessink, B.G.; Ramaekers, G.; van Rijn, L.C. On the parameterization of the free stream non-linear wave orbital motion in nearshore morphodynamic models. *Coast. Eng.* **2012**, *65*, 56–63. [[CrossRef](#)]
44. Davidson, M.A.; Splinter, K.D.; Turner, I.L. A simple equilibrium model for predicting shoreline change. *Coast. Eng.* **2013**, *73*, 191–202. [[CrossRef](#)]
45. Ruessink, B.G.; Blenkinsopp, C.; Brinkkemper, J.A.; Castelle, B.; Dubarbier, B.; Grasso, F.; Puleo, J.A.; Lanckriet, T. Sandbar and beach-face evolution on a prototype coarse sandy barrier. *Coast. Eng.* **2016**, *113*, 19–32. [[CrossRef](#)]
46. Hughes, S.A. *Physical Models and Laboratory Techniques in Coastal Engineering*; World Scientific: Singapore, 1993; Volume 7.
47. Van Rijn, L.C.; Tonnon, P.K.; Sanchez-Arcilla, A.; Cáceres, I.; Grüne, J. Scaling laws for beach and dune erosion processes. *Coast. Eng.* **2011**, *58*, 623–636. [[CrossRef](#)]
48. Larson, M.; Kraus, N.C.; Sunamura, T. Beach profile change: Morphology, transport rate, and numerical simulation. *Coast. Eng.* **1988**, *96*, 1295–1309. [[CrossRef](#)]

**Disclaimer/Publisher's Note:** The statements, opinions and data contained in all publications are solely those of the individual author(s) and contributor(s) and not of MDPI and/or the editor(s). MDPI and/or the editor(s) disclaim responsibility for any injury to people or property resulting from any ideas, methods, instructions or products referred to in the content.